Monitoring the therapeutic efficacy of CA4P in the rabbit VX2 liver tumor using dynamic contrast-enhanced MRI

Tianzhuang Han

Qingqing Duan

Rong Yang

Yuzhe Wang

Huabin Yin

Fanhua Meng

Yongjuan Liu

Ting Qian

PURPOSE

The present work aims to evaluate whether dynamic contrast-enhanced magnetic resonance imaging (DCE-MRI) can monitor the blocking effect of combretastatin-A4-phosphate (CA4P) on microvessels and assess the therapeutic efficacy.

METHODS

Forty rabbits were implanted VX2 tumor specimens. Two weeks later, serial MRI (T1-weighted imaging, T2-weighted imaging, and DCE) were performed at 0 h, 4 h, 24 h, 3 days, and 7 days after CA4P (10 mg/kg) or saline treatment. The parameters of DCE (K^{trans}, K_{ep}, V_e and iAUC60) enhancement of tumor portions were measured. Then all tumor samples were stained to count microvessel density (MVD). Finally, two-way repeated measures ANOVA was used to analyze the difference between and within groups. Correlation between the DCE parameters and MVD was analyzed by using the Pearson correlation and Spearman rank correlation.

RESULTS

K^{trans} and iAUC60 values at 4 h after CA4P treatment were significantly lower than those in the control group (D-value: -0.133 min^{-1}, 95%CI: -0.169 to -0.097 min^{-1}, F= 59.109, $p < 0.001$ for K^{trans}; D-value: -10.533 mmol/s, 95%CI: -17.147 to -3.919 mmol/s, F= 11.110, and $p = 0.003$ for iAUC60). In the CA4P group, K^{trans} and iAUC60 reached the minimum values at 4 h, and both parameters showed significant difference between 4 h and other time points (all $p < 0.01$). Seven-day values of K^{trans} (r=0.532, $p = 0.016$ and r=0.681, $p = 0.001$, respectively) and iAUC60 (r=0.580, $p = 0.007$ and r=0.568, $p = 0.009$, respectively) showed correlation with MVD in both groups, while K_{ep} and V_e did not show correlation with MVD ($p > 0.05$).

CONCLUSION

The blocking effect of microvessels after CA4P treatment can be evaluated by DCE-MRI, and the parameters of quantitative K^{trans} and semi- quantitative iAUC60 can assess the change in tumor angiogenesis noninvasively.

H epatocellular carcinoma (HCC) has the third highest mortality rate worldwide among cancers (1). Although the 5-year survival rate can reach up to 70% of HCC patients by surgical operation, only less than 30% are suitable for surgery. Transarterial chemoembolization (TACE) treated tumors can stimulate angiogenesis and require repeated treatment (2). As HCC is generally hypervascular, vascular targeting strategies can be used to improve the 5-year survival rate (3).

There are two kinds of tumor vascular targeted agents (4): angiogenesis inhibitors (AIs) and vascular disrupting agents (VDAs). AIs can prevent the formation of new blood vessels by inhibiting angiogenesis. VDAs can damage the tumor endothelium directly, shutdown vascular development rapidly and selectively and cause tumor cell ischemia; tumor vascular shutdown occurs within 1 h of administration, and lasts for 24 hours (5, 6). Combretastatin A-4-phosphate (CA4P) is a new-style VDA that progressed into clinical trial stage (7–9).

The vascular disrupting effects of VDAs can be assessed by microvessel density (MVD), which is the "gold standard" measurement to evaluate angiogenesis. However, the invasiveness of MVD measurement limits its use (10).

During the development of targeted treatments, imaging plays an important role in monitoring the treatment efficacy against malignant tumors [11]. Although change in tumor size may not be a reliable method to measure treatment efficacy, plenty of imaging sequences have been developed to overcome the drawbacks of traditional efficacy assessments by size measurement [12–14].

DCE-MRI could reflect the microvascular structure and function indirectly, noninvasively and quantitatively, and it has been widely applied to predict and evaluate the treatment response [15]. DCE-MRI is expected to be useful in evaluating early vascular disrupting efficacy after CA4P administration. But studies focusing on the changes of DCE parameters at different time points after CA4P administration in the VX2 rabbits have been scarce [16–18]. The VX2 liver tumor is supplied by liver artery which is similar with high-grade human HCC, and can be used to simulate the microenvironment of human HCC [19].

In this study, we aimed to investigate whether quantitative parameters in DCE-MRI can monitor the change in microvasculature of liver tumors at different time points after CA4P treatment.

Methods

This study was approved by the ethics committee of the local institution and complies with the guidelines for use of laboratory animals in Fudan university (Laboratory Animal Use License: SYXK 2013-0087).

VX2 liver tumor model

Tumor-bearing rabbits weighed between 2.2 and 2.8 kg. The VX2 tumor cells recovered from liquid nitrogen were injected into the hind limb muscles to build the models. Once the size of the tumor reached about 3 cm, they were removed by aseptic operation and incised into 1–2 mm^3 cubes. Zoletil 50 (tiletamine hydrochloride zolazepam hydrochloride, Virbac S.A, 5 mg/kg) was injected into muscles to sedate the 40 New Zealand white rabbits. Then, the tumor tissue were implanted in the left lobe of the liver by percutaneous puncture under CT guidance. Finally, 29 VX2 liver tumor models were built successfully.

Experimental protocol

The rabbits models were divided into CA4P and control groups (20 rabbits per group). Fosbretabulin disodium (combretastatin A4 phosphate, Target Mol, 10 mg/kg) [20] or saline was administered to the rabbits by ear marginal vein injection after baseline MRI; follow-up MRI scans were performed at 4 h, 24 h, 3 days, and 7 days after CA4P or saline administration. All rabbits were euthanized at the end of the experiment.

MRI acquisition

After 2 weeks, imaging was performed using a 3.0 T MRI scanner (Magnetom Skyra, Siemens Healthineers) with a special coil for rabbits (CG-RBC18-H300-AS, Shanghai Chen Guang Medical Technologies Company Limited). Liver tumor models were deemed successful based on the following criteria: mass located in the left lobe of liver; necrosis <30%; average diameter of approximately 2 cm. Rabbits were sedated and kept in a supine position. A deep anesthetic was administered and medical towels were wrapped around the abdomen of rabbits to reduce the influence of free breathing.

The basic sequence and T1 map was acquired first. Then, five frames of unenhanced images were acquired, following 1 mL Gd-DTPA (at a dose of 0.2 mmol/kg body weight) injected into the left or right marginal ear vein with a bolus of 2 mL/s by the automated injector (C1213D005X, Mallinckrodt). A total of 60 measurements were acquired. Table 1 shows the scanning protocols of MRI.

Image analysis

The DCE images were analyzed by Tissue4D workstation (software based on the Tofts model, syngo multimodality workplace, Siemens), according to the following model equation [21]:

$$C_t(t) = K^{trans} \int C_p(\tau) e^{-k_{ep}(t-\tau)} \, d\tau$$

where $C_t(t)$ is the agent concentration at the time t, and $C_p(t)$ is the plasma volume of the agent. K^{trans} is the volume transfer constant between the plasma and the extracellular extravascular space (EES); K_{ep} is the rate constant from the EES to the plasma; V_e is the fraction of the plasma volume; iAUC60 is the dose of the agent taken up by the tumor from injection point until 60 seconds.

The above DCE parameters were measured by two radiologists, who were blinded to the experimental allocation. ROIs were manually drawn on the obvious enhancement areas of the largest slice and the size were about 20 pixels, excluding septa and vessels. Then, the mean values of K^{trans}, K_{ep}, V_e and iAUC60 derived from color-coded parametric maps were obtained. At the same time, we got the volume of the tumor based on the largest slice of T2-weighted image, according to the formula: V=(length × width^2)/2, where length represents the largest dimension of the tumor, and width represents the widest diameter perpendicular to the length [22].

Main points

- DCE-MRI might be used to monitor the efficacy of CA4P at early time points.

- DCE-MRI parameters (K^{trans} and iAUC60) can produce significant changes at 4 h, and there are still differences at 7 days after CA4P treatment.

- K^{trans} and iAUC60 can indirectly monitor the microvessels of the tumor both in the treatment group and the control group.

Table 1. List of MRI scanning parameters

	T1WI	T2WI	T1-MAP	DCE-MRI
Sequence type	GRE	TSE	VIBE	VIBE
Flip angle (°)	70°	145°	6°	15.0°
Field of view (mm)	164	120	120	120
TR/TE (ms)	170/2.24	4000/98	4.70/1.78	4.70/1.78
Number of averages	1	5	1	1
Thickness (mm)	3.0	3.0	3.0	2.50
Slices	22	20	20	20
Acquisition time (min:s)	0:39	3:26	0:10	10:16

T1WI, T1-weighted imaging; T2WI, T2-weighted imaging; T1-MAP, T1 mapping sequence; DCE-MRI, dynamic contrast-enhanced magnetic resonance imaging; GRE, gradient recalled echo; TSE, turbo spin echo; VIBE, volumetric interpolated breath-hold examination; TR, repetition time; TE, echo time.

Histologic analysis

All the rabbits were euthanized after the last MRI scanning. The tumor specimens were fixed in 10% formalin, and embedded in paraffin, then sectioned into 5 μm slides and stained with hematoxylin-eosin-saffron and CD31 (Abcam).

Microvessels were counted using light microscopy (Leica, DM2500) by an experienced pathologist with more than 8 years of experience, who was blinded to the experimental assignment. First, a hot spot indicating higher vessel areas was selected at low magnification (×40), which was matched with the enhancement areas of DCE-MRI images. Then five areas were chosen to count the MVD at high magnification (×200). And finally the average MVD was calculated.

Statistical analysis

We used the SPSS Statistics software (Version 23.0, IBM) to analyze the data. Shapiro-wilk test was used to assess normal distribution. Data were presented as mean ± standard deviation (SD) for normal distribution, while median (min–max) was given for non-normal distribution. Two-way repeated measures ANOVA was used to analyzed the difference between and within groups. The correlations between parameters of DCE-MRI (K^{trans}, K_{ep}, V_e and iAUC60 value) and MVD were quantified with Pearson correlation coefficient and Spearman rank correlation. A p value of < 0.05 was considered to be statistically significant.

Results

Most of the data fulfilled the normal distribution, except K^{trans} of 7 days ($p = 0.006$), V_e of 4 h ($p = 0.006$), and V_e of 24 h ($p = 0.007$) in the control group, with the remaining p values >0.05.

At baseline, 4 h, 24 h, 3 days, and 7 days, the mean tumor volumes were 259.3±49.9 mm³, 264.5±49.2 mm³, 336.6±46.9 mm³, 416.6±46.5 mm³, 484.3±38.5 mm³ in the CA4P group. In the control group, the average tumor volumes were 272.3±34.7 mm³, 313.6±50.5 mm³, 357.2±51.7 mm³, 445.9±18.8 mm³, 516.9±71.6 mm³. The growth trend of tumors in the CA4P group was slower than that in the control group, but the volumes of the two groups did not show significant difference at different time points ($p = 0.570$, $p = 0.10$, $p = 0.390$, $p = 0.160$, and $p = 0.180$).

Two weeks after implantation, the tumor with irregular margin located in the left lobe was found, which showed hypointensity on T1-weighted image and slight hyperintensity on T2-weighted image (Fig. 1).

In our study, ring-enhancement of the rim appeared in DCE imaging in both groups. The time-signal intensity curve (TIC) of the lesion was type III, which showed a rapid uptake followed by reduction in enhancement, the normal tissue was in accordance with type II curves, which showed a gentle ascent initially followed by a plateau (Fig. 1).

Most data fulfilled normal distribution, except the K^{trans} of 7 days ($p = 0.006$), the V_e of 4 h ($p = 0.006$), and the V_e of 24 h ($p = 0.007$) in the control group; all the remaining p values were >0.05. At 4 h, the K^{trans} and iAUC60 in the treatment group were lower than the values in the control group (D-value: -0.133 min⁻¹, 95% CI: -0.169 to -0.097 min⁻¹, F= 59.109, $p < 0.001$ of K^{trans}; D-value: -10.533 mmol/s, 95% CI: -17.147 to -3.919 mmol/s, F= 11.110, $p = 0.003$). K_{ep} and V_e did not show significant differences ($p =$ 0.712 and $p = 0.937$). At other time points, the parameters did not show any significant differences (all $p > 0.05$) (Table 2 and Fig. 2).

The K^{trans} and iAUC60 of the treatment group showed an obvious trend of "decrease-increase". Moreover, the values of K^{trans} and iAUC60 rapidly decreased at 4 h and slowly increased at 24 h, 3 days, 7 days. There were significant differences between 4 h and other time points for K^{trans} and iAUC60 in the treatment group ($p = 0.001$, $p = 0.004$, $p = 0.001$ and $p < 0.001$ for K^{trans}, $p = 0.003$, $p = 0.023$, $p < 0.001$ and $p < 0.001$ for iAUC60). K_{ep} and V_e values did not show this characteristic (all $p = 1.000$) (Tables 3–5 and Fig. 2).

The tumor appeared to have a fish-like form by naked eye. On H&E staining, the viable tissues were distributed in the periphery with large and hyperchromatic nuclei, and some coagulative necrosis accompanied with a lot of inflammatory cells could be seen in the treatment group (Figs. 3 and 4).
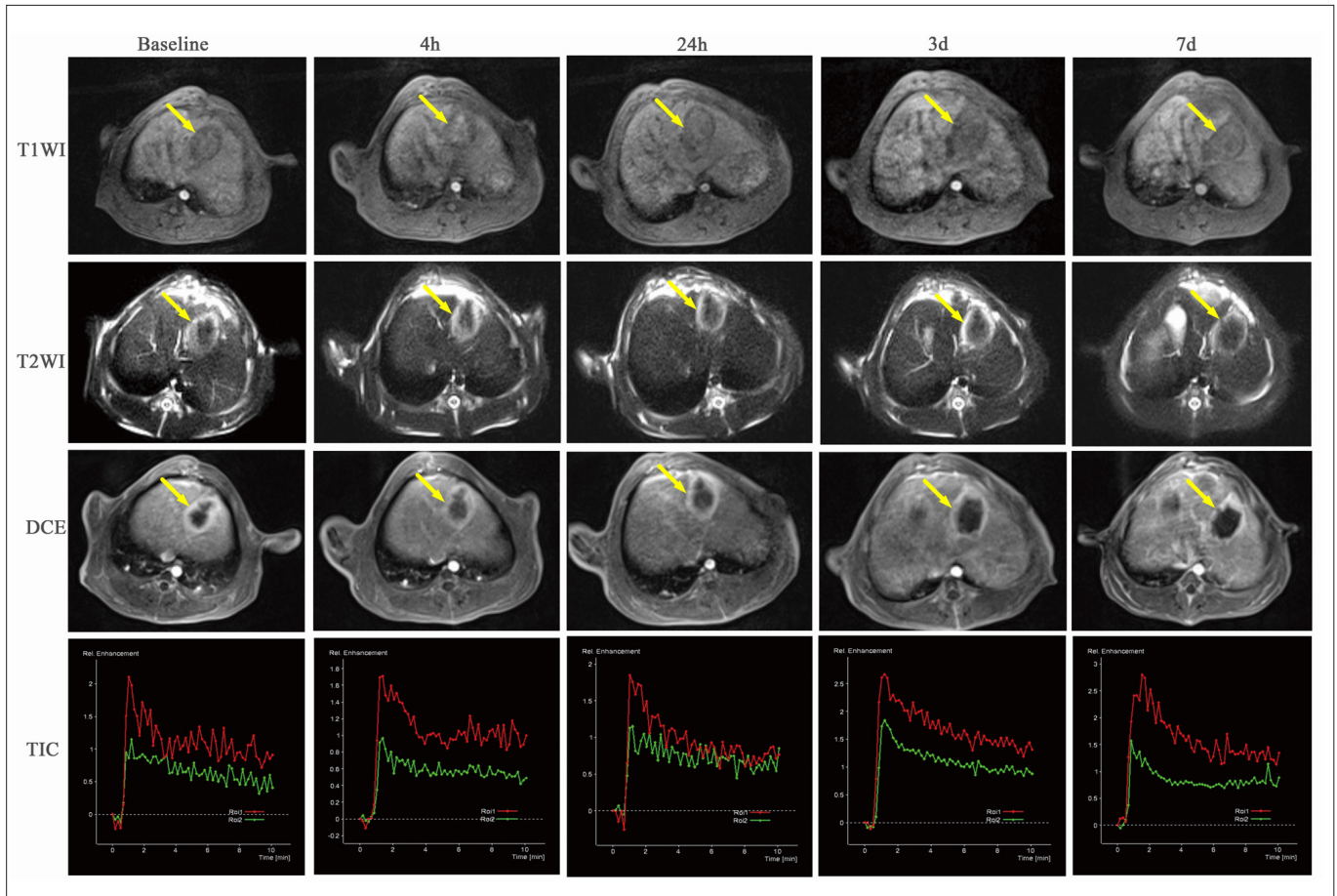
Table 2. DCE-MRI quantitative parameters at different time points between the treatment group and the control group

Parameters	Time points	Treatment group	Control group	p
K^{trans}	Baseline	0.327±0.106	0.339±0.085	0.639
	4 hours	0.217±0.078	0.349±0.070	<0.001
	24 hours	0.323±0.113	0.353±0.082	0.311
	3 days	0.329±0.093	0.341±0.077	0.666
	7 days	0.385±0.081	0.355 (0.240–0.450)	0.197
K_{ep}	Baseline	0.589±0.132	0.597±0.135	0.862
	4 hours	0.574±0.143	0.558±0.150	0.712
	24 hours	0.590±0.148	0.563±0.125	0.534
	3 days	0.587±0.131	0.574±0.118	0.704
	7 days	0.601±0.102	0.581±0.162	0.635
V_e	Baseline	0.600±0.213	0.589±0.115	0.821
	4 hours	0.578±0.197	0.573 (0.390–0.910)	0.937
	24 hours	0.579±0.149	0.586 (0.390–0.950)	0.871
	3 days	0.592±0.129	0.584±0.143	0.842
	7 days	0.586±0.136	0.606±0.120	0.684
iAUC	Baseline	33.118±12.094	32.147±8.286	0.778
	4 hours	22.404±6.670	32.936±9.551	0.003
	24 hours	29.419±10.300	33.698±7.959	0.131
	3 days	30.907±8.958	35.801±8.039	0.102
	7 days	37.225±8.625	37.865±9.763	0.805

Data were presented as mean ± standard deviation (SD) for normal distribution, median (min–max) for non-normal distribution.
Bonferroni post hoc test was used and $p < 0.05$ was considered statistically significant.
DCE-MRI, dynamic contrast-enhanced magnetic resonance imaging; K^{trans}, volume transfer constant; K_{ep}, reflux rate constant; V_e, volume fraction of the extravascular extracellular space; iAUC, initial area under the contrast concentration-time curve.

Figure 1. Representative T1-weighted, T2-weighted, DCE, and TIC imaging at different time points. The VX2 liver tumors appears hypointense on T1-weighted image and hyperintense on T2-weighted image with a spherical or oval shape, and the ring enhancement of the rim appears in DCE imaging *(arrow)*. The TIC demonstrates rapid increase in signal intensity of the tumor (ROI 1, *red*), and the peak intensity is higher than that of the normal tumor (ROI 2, *green*). K^{trans}, K_{ep}, V_e and iAUC60 values were measured during the imaging.
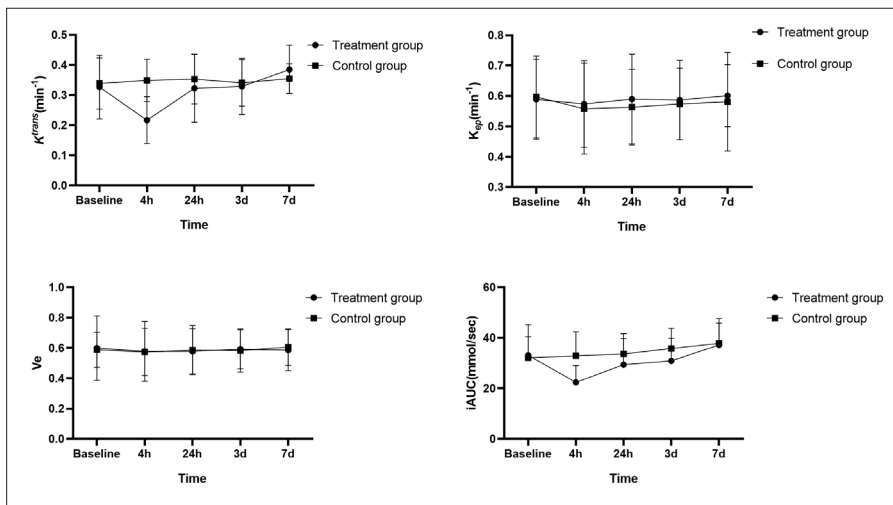

Figure 2. Serial measurements of the K^{trans}, K_{ep}, V_e and iAUC60 in both groups at different time points. K^{trans} and iAUC60 showed rapid decrease at 4 h and slow increase at 24 h, 3 days, and 7 days. This characteristic did not exist in the values of K_{ep} and V_e.

MVD was counted according to Weidner et al. (23). Any CD31 positive endothelial cells or clusters or branches were considered as individual microvessels, except for the large vessels with more than eight red blood cells in the lumen. More stained blood vessels could be seen in the control group than in the treatment group (Figs. 5 and 6).

In the treatment group, K^{trans} and iAUC60 of the viable tissues at 7 days showed a positive correlation with MVD (r=0.532, p = 0.016 for K^{trans}, r=0.580, p = 0.007 for iAUC60, respectively), whereas K_{ep} and V_e did not show a correlation with MVD (r= -0.371, p = 0.108 for K_{ep}, r= -0.055, p = 0.818 for V_e, respectively) (Fig. 7).

In the control group, K^{trans} and iAUC60 of the viable tissues at 7 days also showed a positive correlation with MVD (r=0.681, p = 0.001 for K^{trans}, r=0.568, p = 0.009 for iAUC60, respectively), while K_{ep} and V_e did not show a correlation with MVD (r= -0.416, p = 0.068 for K_{ep}, r=0.336, p = 0.148 for V_e, respectively) (Table 6 and Fig. 7).

Discussion

The present work demonstrated that DCE-MRI is able to monitor noninvasively the blocking effect on microvessels after CA4P administration in the early stage, and there is positive correlation between two quantitative parameters of DCE-MRI (K^{trans} and iAUC60) and MVD.

Table 3. Repeated measure ANOVA of K^{trans} and iAUC

	Time*Group effect		Time effect		Group effect in the control group		Group effect in the CA4P group	
	F	p	F	p	F	p	F	p
K^{trans}	$F_{(4, 76)}= 5.818$	<0.001	F=59.109	<0.001	$F_{(4, 76)}= 0.251$	0.908	$F_{(2.272, 43.163)}= 11.512$	<0.001
iAUC	$F_{(4, 76)}= 8.573$	<0.001	F=11.110	0.003	$F_{(4, 76)}= 0.326$	0.018	$F_{(2.806, 53.320)}= 10.346$	<0.001

$p < 0.05$ is considered statistically significant.

Table 4. Repeated measure ANOVA of K_{ep} and V_e

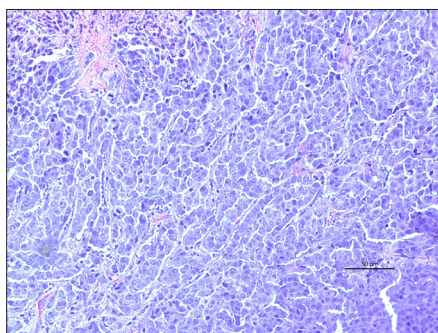|	Time*Group effect		Time effect		Group effect	
	F	p	F	p	F	p
K_{ep}	$F_{(2.718, 51.645)}= 0.122$	0.935	$F_{(1.749, 33.234)} = 0.446$	0.618	$F_{(1, 19)}= 0.043$	0.837
V_e	$F_{(2.257, 42.877)}= 0.253$	0.803	$F_{(2.064, 39.212)} = 0.045$	0.960	$F_{(1, 19)}= 0.457$	0.507

$p < 0.05$ was considered statistically significant.

Figure 3. Hematoxylin-eosin (H&E) staining in the treatment group (magnification ×200). Irregular cell morphology and deeply stained nuclei were seen in the viable portions of the tumor. Some coagulative necrosis accompanied by a lot of inflammatory cells can also be seen.
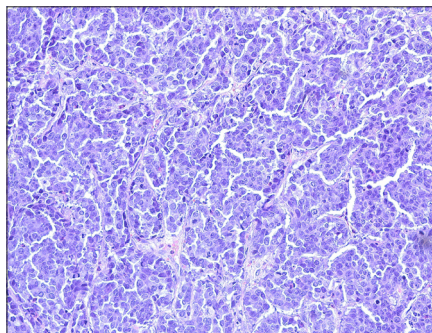

Figure 4. H&E staining in the control group (magnification ×200). Large and hyperchromatic nuclei were seen in the tumor.
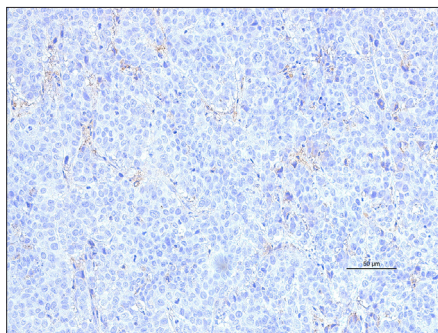

Figure 5. Immunohistochemical anti-CD31-stained tumor section in the treatment group (magnification ×200). CD31-positive vessels appear brown.
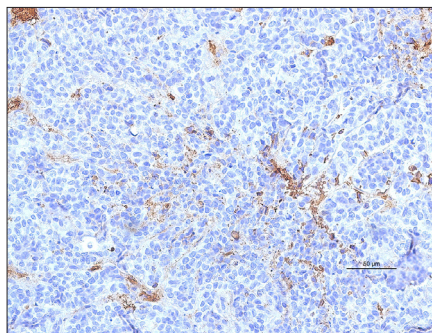

Figure 6. Immunohistochemical anti-CD31-stained tumor section in the control group (magnification ×200). Endothelial cells appear brown. More stained blood vessels can be seen in the control group than in the treatment group.

MRI is the common method for noninvasive monitoring of treatment efficacy (24, 25). Quantitative analysis on DCE-MRI, based on higher neoangiogenesis and vascular permeability in malignant lesions and a pharmacokinetic model and microcirculation parameters (26), has been widely used in assessment of antivascular treatments (27, 28).

CA4P is the prototypical member of the combretastatin class and is the first VDA to enter clinical trials (9, 29). CA4P depolymerizes the microtubules of endothelial cells, leading to endothelial cell detachment from the blood vessels, changes in tumor vascular morphology, and blockage of the vascular lumen. This pathological mechanism has quick effect, is persistent over a short time, and the microenvironmental changes predate the morphological changes.

With the development of vascular targeted therapies, multiple acquisitions of the tumor perfusion data are necessary to find the best onset time and to guide the subsequent treatment (30). The retention problem of the agent in kidney is often mentioned during DCE acquisition, especially in patients with poor kidney function. CA4P could improve the retention of Gd-DTPA in the tumor (31) and reduce the excretion from kidney, which is important for clinical outcome.

Response Evaluation Criteria in Solid Tumors (RECIST) as the traditional criteria for cancer treatment cannot be used to measure tumor response to CA4P. This is mainly because all tumors showed growth, even in the treatment groups treated with CA4P, indicating progressive disease. These results have been predicted, as CA4P is not expected to reduce tumor size, in contrast to conventional chemotherapy, and VX2 tumors are known to grow aggressively. The rim of the tumor showed weaker response than the center, which made the rim of the tumor thicker, probably increasing tumor volume. However, the specific mechanism of the phenomenon remains unclear (32).

There are three types of TIC (33). Type I was defined as mild ascent without a plateau, Type II was described as gentle ascent initially followed by a plateau and Type III as relatively rapid uptake followed by reduction in enhancement. In our study, all viable tumor tissue presented a type III TIC. The method was described by Kuhl et al. (34). They reported a diagnostic accuracy of 86% for the Type III curves in diagnosing malignant breast lesion. Malek et al. (26) got the same conclusion that Type III TIC confirmed the malignancy tumor of adnexal masses.
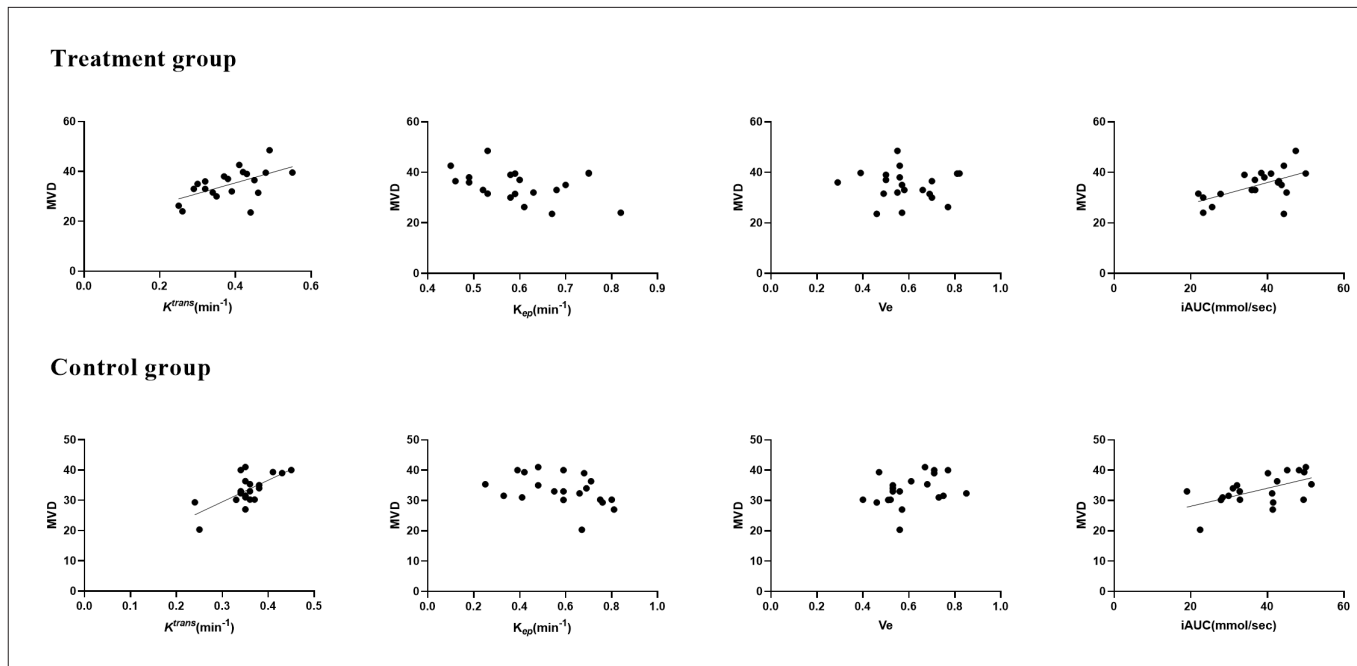
Figure 7. Scatter plot shows the correlation between the K^{trans}, K_{ep}, V_e and iAUC60 values at 7 days and MVD in both groups. A linear relationship was observed between K^{trans}, iAUC60 and MVD (r= 0.532, p = 0.016 for K^{trans}, r= 0.580, p = 0.007 for iAUC60, in the treatment group; r= 0.681, p = 0.001 for K^{trans}, r= 0.568, p = 0.009 for iAUC60, in the control group).

Table 5. D-values of the average values (95% CI) and p values of K^{trans} and iAUC in the treatment group at different time points

Parameter	D-values of the average values (95% CI)			
	4 hours	24 hours	3 days	7 days
K^{trans}				
Baseline	0.111* (0.041 to 0.181)	0.005 (-0.100 to 0.109)	-0.002 (-0.109 to 0.105)	-0.057 (-0.161 to 0.047)
4 hours		-0.106* (-0.184 to -0.028)	-0.113* (-0.185 to -0.041)	-0.168* (-0.243 to -0.093)
24 hours			-0.007 (-0.063 to 0.049)	-0.062 (-0.135 to 0.011)
3 days				-0.055* (-0.098 to -0.012)
7 days				
iAUC				
Baseline	10.714* (3.143 to 18.286)	3.698 (-5.492 to 12.889)	2.210 (-7.276 to 11.696)	-4.107 (-14.045 to 5.831)
4 hours		-7.016* (-13.361 to -0.671)	-8.504* (-13.396 to -3.613)	-14.821* (-22.252 to -7.391)
24 hours			-1.488 (-6.682 to 3.706)	-7.805* (-15.516 to -0.095)
3 days				-6.317 (-12.827 to 0.192)
7 days				

K^{trans}, volume transfer constant; K_{ep}, reflux rate constant; V_e, volume fraction of the extravascular extracellular space; iAUC, initial area under the contrast concentration-time curve; CI, confidence interval.
* p < 0.05, which is considered statistically significant.

In the CA4P group, K^{trans} and iAUC60 values at 4 h were significantly lower than those before treatment, and then gradually increased. There were significant differences between 4 h and other time points (p < 0.05), which demonstrated that DCE-MRI quantitatively reflected the blockage of tumor blood vessels. Meanwhile, our findings provide an explanation for the mechanism of CA4P (35). CA4P has a strong blocking effect on tumor blood vessels within 12 hours after administration, which is proportional to the concentration of CA4P in blood. The specific intensity of the effect needs to be further studied through hemodynamic studies combined with imaging examinations at different time points. Our previous research (12) also demonstrated that K^{trans} and iAUC60 can be used to evaluate the effectiveness after treatment. A study by Park et al. (36) showed a similar result. Other previous studies obtained different results. Wu et al. (25) concluded that K^{trans}, K_{ep}, and iAUC60 can monitor radiotherapy-induced tissue changes in localized prostate cancer. Liang et al. (28) found that CD31 positive staining rate had

Table 6. Correlation between DCE-MRI quantitative parameters and MVD at 7 days

Group	Parameters	MVD	
		r	p
Treatment group	K^{trans}	0.532	0.016
	K^{ep}	-0.371	0.108
	V^e	-0.055	0.818
	iAUC	0.580	0.007
Control group	K^{trans}	0.681	0.001
	K_{ep}	-0.416	0.068
	V_e	0.336	0.148
	iAUC	0.568	0.009

All data were tested with Pearson correlation coefficient and Spearman rank correlation.
MVD counts was 34.819±6.202 in the treatment group and 33.422±5.102 in the control group.
$p < 0.05$ was considered statistically significant.

the strongest correlations with K^{trans} values, followed by AUC180, V_e and K_{ep} values after bevacizumab treatment. Moreover, they concluded that DCE-MRI is useful for monitoring tumor microenvironment changes during anti-angiogenesis therapy. It is largely due to the nuance of different therapy method and the lack of standardization in the field may be one reason.

The K^{trans} and iAUC60 of the viable tissues of the control groups showed a positive correlation with MVD, which showed that K^{trans} and iAUC60 were correlated with angiogenesis. The same conclusion was drawn in the treatment group as well, which indicated that K^{trans} and iAUC60 also represented the microvascular changes after CA4P administration. A similar conclusion had also been found in other reports (37, 38). At the same time, in previous studies, there have been controversial conclusions. A study of HCC patients (38) showed that K_{ep} and V_e were significantly related with tumor MVD. A significant correlation between K^{trans}, K_{ep} and MVD on day 21 after the rats brain glioma models built was found by Hou et al. (40). The reasons are still unclear for these arguments, but one potential explanation is the difference in tumor type (41).

There are limitations to this study. First, for the selection of ROI, only the axial imaging of the tumor was measured, which is not representative of the whole tumor. Second, since the histologic features were only evaluated at 7 days after treatment, the histologic findings of early times, such as 4 hours after CA4P treatment, were not assessed. Third, there was potential bias due to the limited number of animals in each group. The correlation between pathology findings and MRI parameters still requires more research.

In conclusion, our animal study suggests that DCE-MRI might be used to monitor the tumor response of CA4P at early time points. The DCE-MRI parameters (K^{trans} and iAUC60) can produce significant changes at 4 h, and there are still differences at 7 days after CA4P treatment, which is important for clinical outcome. Therefore, DCE-MRI may be a promising tool for monitoring the CA4P effect.

Conflict of interest disclosure
The authors declared no conflicts of interest.

References
1. Arif-Tiwari H, Kalb B, Chundru S, et al. MRI of hepatocellular carcinoma: an update of current practices. Diagn Interv Radiol 2014; 20:209–221. [Crossref]
2. Liu K, Zhang X, Xu W, et al. Targeting the vasculature in hepatocellular carcinoma treatment: Starving versus normalizing blood supply. Clin Transl Gastroenterol 2017; 8:e98. [Crossref]
3. Liu Y, De Keyzer F, Wang Y, et al. The first study on therapeutic efficacies of a vascular disrupting agent CA4P among primary hepatocellular carcinomas with a full spectrum of differentiation and vascularity: Correlation of MRI-microangiography-histopathology in rats. Int J Cancer 2018; 143:1817–1828. [Crossref]
4. Eichten A, Adler AP, Cooper B, et al. Rapid decrease in tumor perfusion following VEGF blockade predicts long-term tumor growth inhibition in preclinical tumor models. Angiogenesis 2013; 16:429–441. [Crossref]
5. Chase DM, Chaplin DJ, Monk BJ. The development and use of vascular targeted therapy in ovarian cancer. Gynecol Oncol 2017; 145:393–406. [Crossref]
6. Chaplin DJ, Pettit GR, Parkins CS, et al. Antivascular approaches to solid tumour therapy: evaluation of tubulin binding agents. Br J Cancer 1996; 27 (Suppl):S86–S88.
7. Garon EB, Neidhart JD, Gabrail NY, et al. A randomized phase II trial of the tumor vascular disrupting agent CA4P (fosbretabulin tromethamine) with carboplatin, paclitaxel, and bevacizumab in advanced nonsquamous non-small-cell lung cancer. Onco Targets Ther 2016; 9:7275–7283. [Crossref]
8. Liu P, Qin Y, Wu L, et al. A phase I clinical trial assessing the safety and tolerability of combretastatin A4 phosphate injections. Anticancer Drugs 2014; 25:462–471. [Crossref]
9. Shi C, Liu D, Xiao Z, et al. Monitoring tumor response to antivascular therapy using non-contrast intravoxel incoherent motion diffusion-weighted MRI. Cancer Res 2017; 77:3491–3501. [Crossref]
10. Seshadri M, De Keyzer F, Wang Y, et al. Activity of the vascular-disrupting agent 5,6-dimethylxanthenone-4-acetic acid against human head and neck carcinoma xenografts. Neoplasia 2006; 8:534–542. [Crossref]
11. Lee Y, Lee SS, Cheong H, et al. Intravoxel incoherent motion MRI for monitoring the therapeutic response of hepatocellular carcinoma to sorafenib treatment in mouse xenograft tumor models. Acta Radiol 2017; 58:1045–1053. [Crossref]
12. Qian T, Chen MZ, Gao F, et al. Diffusion-weighted magnetic resonance imaging to evaluate microvascular density after transarterial embolization ablation in a rabbit VX2 liver tumor model[J]. Magnetic Resonance Imaging, 2014,32:1052-1057. [Crossref]
13. Pan J, Zhu S, Huang J, et al. Monitoring the process of endostar-induced tumor vascular normalization by non-contrast intravoxel incoherent motion diffusion-weighted MRI. Frontier Oncol 2018; 8:524. [Crossref]
14. Chen J, Qian T, Zhang H, et al. Combining dynamic contrast enhanced magnetic resonance imaging and microvessel density to assess the angiogenesis after PEI in a rabbit VX2 liver tumor model[J]. Magnetic Resonance Imaging, 2016,34:177-182. [Crossref]
15. Chen QH, Wang XY, Zhang B, et al. Quantitative dynamic contrast enhancement MR imaging parameters in the prediction and evaluation of the treatment response of malignant sinonasal tumors to chemotherapy: a preliminary result. Zhonghua Yi Xue Za Zhi 2019; 99:1773–1777.
16. Joo I, Lee JM, Grimm R, et al. Monitoring vascular disrupting therapy in a rabbit liver tumor model: relationship between tumor perfusion parameters at IVIM diffusion-weighted MR imaging and those at dynamic contrast-enhanced MR imaging. Radiology 2016; 278:104–113. [Crossref]
17. Salmon BA, Salmon HW, Siemann DW. Monitoring the treatment efficacy of the vascular disrupting agent CA4P. Eur J Cancer 2007; 43:1622–1629. [Crossref]
18. Shao H, Ni Y, Zhang J, et al. Dynamic contrast-enhanced and diffusion-weighted magnetic resonance imaging noninvasive evaluation of vascular disrupting treatment on rabbit liver tumors. PLoS One 2013; 8:e82649. [Crossref]
19. Hoekstra LT, van Lienden KP, Verheij J, et al. Enhanced tumor growth after portal vein embolization in a rabbit tumor model. J Surg Res 2013; 180:89–96. [Crossref]

20. Abma E, Daminet S, Smets P, et al. Combretastatin A4-phosphate and its potential in veterinary oncology: a review. Vet Comp Oncol 2017; 15:184–193. [Crossref]

21. Tofts PS, Brix G, Buckley DL, et al. Estimating kinetic parameters from dynamic contrast-enhanced T(1)-weighted MRI of a diffusable tracer: standardized quantities and symbols. J Magn Reson Imaging 1999; 10:223–232.

22. Naito S, von Eschenbach AC, Giavazzi R, et al. Growth and metastasis of tumor cells isolated from a human renal cell carcinoma implanted into different organs of nude mice. Cancer Res 1986; 46:4109–4115.

23. Weidner N. Current pathologic methods for measuring intratumoral microvessel density within breast carcinoma and other solid tumors. Breast Cancer Res Treat 1995; 36:169–180. [Crossref]

24. Hussein RS, Tantawy W, Abbas YA. MRI assessment of hepatocellular carcinoma after locoregional therapy. Insights Imaging 2019; 10:8. [Crossref]

25. Wu X, Reinikainen P, Kapanen M, et al. Monitoring radiotherapy induced tissue changes in localized prostate cancer by multi-parametric magnetic resonance imaging (MP-MRI). Diagn Interv Imaging 2019; 100:699–708. [Crossref]

26. Malek M, Oghabian Z, Tabibian E, et al. Comparison of qualitative (time intensity curve analysis), semi-quantitative, and quantitative multi-phase 3T DCEMRI parameters as predictors of malignancy in adnexal. Asian Pac J Cancer Prev 2019; 20:1603–1611. [Crossref]

27. Jun W, Cong W, Xianxin X, et al. Meta-analysis of quantitative dynamic contrast-enhanced MRI for the assessment of neoadjuvant chemotherapy in breast cancer. Am Surg 2019; 85:645–653. [Crossref]

28. Liang J, Cheng Q, Huang J, et al. Monitoring tumour microenvironment changes during anti-angiogenesis therapy using functional MRI. Angiogenesis 2019; 22:457–470. [Crossref]

29. Siemann DW, Chaplin DJ, Walicke PA. A review and update of the current status of the vasculature-disabling agent combretastatin-A4 phosphate (CA4P). Expert Opin Investig Drugs 2009; 18:189–197. [Crossref]

30. Zweifel M, Padhani AR. Perfusion MRI in the early clinical development of antivascular drugs: decorations or decision making tools? Eur J Nucl Med Mol Imaging 2010; 37:S164–S182. [Crossref]

31. Gao M, Yao N, Huang D, et al. Trapping effect on a small molecular drug with vascular-disrupting agent CA4P in rodent H22 hepatic tumor model: in vivo magnetic resonance imaging and postmortem inductively coupled plasma atomic emission spectroscopy. J Drug Targeting 2015; 23:436–443. [Crossref]

32. Joo I, Lee JM, Han JK, et al. Intravoxel incoherent motion diffusion-weighted MR imaging for monitoring the therapeutic efficacy of the vascular disrupting agent CKD-516 in rabbit VX2 liver tumors. Radiology 2014; 272:417–426. [Crossref]

33. Thomassin-Naggara I, Balvay D, Rockall A, et al. Added value of assessing adnexal masses with advanced MRI techniques. Biomed Res Int 2015; 2015:785206. [Crossref]

34. Kuhl CK, Mielcareck P, Klaschik S, et al. Dynamic breast MR imaging: are signal intensity time course data useful for differential diagnosis of enhancing lesions? Radiology 1999; 211:101–110. [Crossref]

35. Liu Y, De Keyzer F, Feng Y, et al. Intra-individual comparison of therapeutic responses to vascular disrupting agent CA4P between rodent primary and secondary liver cancers. World J Gastroenterol 2018; 24:2710–2721. [Crossref]

36. Park HS, Han JK, Lee JM, et al. Dynamic contrast-enhanced MRI using a macromolecular MR contrast agent (P792): evaluation of antivascular drug effect in a rabbit VX2 liver tumor model. Korean J Radiol 2015; 16:1029–1037. [Crossref]

37. Luo J, Zhou K, Zhang B, et al. Intravoxel incoherent motion diffusion-weighted imaging for evaluation of the cell density and angiogenesis of cirrhosis-related nodules in an experimental rat model: comparison and correlation with dynamic contrast-enhanced MRI. J Magn Reson Imaging 2019; 5:812–823. [Crossref]

38. Yang RM, Zou Y, Huang DP, et al. In vivo assessment of the vascular disrupting effect of M410 by DCE-MRI biomarker in a rabbit model of liver tumor. Oncol Rep 2014; 32:709–715. [Crossref]

39. Chen J, Chen C, Xia C, et al. Quantitative free-breathing dynamic contrast-enhanced MRI in hepatocellular carcinoma using gadoxetic acid: correlations with Ki67 proliferation status, histological grades, and microvascular density. Abdom Radiol (NY) 2018; 43:1393–1403. [Crossref]

40. Hou W, Xue Y, Tang W, et al. Evaluation of tumor hypoxia in C6 glioma rat model with dynamic contrast-enhanced magnetic resonance imaging. Acad Radiol 2019; 26:e224–e232. [Crossref]

41. Meyer HJ, Wienke A, Surov A. Correlation between Ktrans and microvessel density in different tumors: a meta-analysis. Anticancer Res 2018; 38:2945–2950. [Crossref]